Adrenal Imaging with ^{131}I-Adosterol (NCL-6-^{131}I) by Diverging and Pinhole Methods

II. Analysis of Abnormal Adrenal Images

Masayuki Nakajo

Department of Radiology, Kagoshima University School of Medicine, Kagoshima 890, Japan
(Director: Prof. S. Shinohara)

Research Code No.: 730

Key Words: *Adrenal imaging, ^{131}I-Adosterol, Adrenal disease, Diverging collimator, Pinhole collimator*

ダィバージング及びピンホール法による ^{131}I-Adosterol (NCL-6-^{131}I) 副腎シンチグラフィ

Ⅱ. 異常副腎像の解析

鹿児島大学医学部放射線医学教室（主任：篠原慎治教授）
中　條　政　敬

（昭和56年5月19日受付）
（昭和56年7月13日最終原稿受付）

種々の副腎疾患43例（アルドステロン症18例，クッシング症候群7例，副腎性器症候群2例，褐色細胞腫3例とその他13例），副腎近傍腫瘍4例と卵巣男化胚細胞腫1例の計48例の^{131}I-Adosterolによる diverging 像と pinhole 像が解析され，各疾患の imaging pattern が検討された．この解析検討より副腎像の pattern 分類が試みられた．また文献的考察も加え，種々の pattern を生ずる三原則（1．皮質腫瘍への集積，2．内因性ACTHとの関連性，3．非皮質腫瘍への非集積）と幾つかの附加的因子が帰納できた．baseline imaging での副腎腫瘍側診断率は，diverging 像での両副腎の activity の比較診断では70%（21/30），pinhole 像による形態診断では97%（28/29）であり，pinhole 像での診断が優れていた．両体位副腎左右摂取比に関しては，副腎腫瘍例の86%（25/29）で高ないし低 net counts 側が一致したが，正常上限値を越える値は右高群で38%（6/16），左高群では92%（12/13）であり，原発性アルドステロン症では右高群で9例中1例，左高群では8例中7例に得られた．従ってこの比は左高群では正常と異常の解離は大であったが，右高群ではそれらの overlap が大であり，副腎腫瘍，特に原発性アルドステロン症の患側決定には信頼性の高い指標とはなり得なかった．15例の摘出副腎の組織濃度に関する検討がなされたが，6例の原発性アルドステロン症では，その摘出副腎の摂取率は平均0.82%（0.60～1.38）であった．また

Presented, in part, at the 19th Annual Meeting of the Japanese Society of Nuclear Medicine, Tokyo, Nov. 26-29, 1979.

その% dose/g は腺腫で平均0.17 (0.11—0.27), 腺腫近傍組織で0.077 (0.050—0.097) であり, Seabold らの ^{131}I-19-iodocholesterol の値と比し, 各々6倍, 3倍であった. 各副腎毎に撮像する Pinhole 法での副腎像は, 他のコリメータ像より高解像であり, 撮像時間が延長する欠点を除けば, 本法はガンマカメラを有する施設ではどこでも簡単に施行可能で, 詳細な診断情報を提供する副腎撮像法として推奨できると考えられた.

Introduction

The advent of ^{131}I-19-iodocholesterol in 1970[1] and the more recent superior agent, ^{131}I-Adosterol (NCL-6-^{131}I) or ^{131}I-NP-59 in 1975[2][3] enabled adrenal disorders to be assessed by the scintigraphic method. Until now, many papers have been published concerning the significance of adrenal imaging with these agents in the diagnosis of patients with various adrenal disorders[4]-[20]. The diagnostic criteria were mainly based on the degree of concentration of the tracer in the adrenals or the comparison of radioactivity between both glands and were not based on their morphological aspects. This may be due to the relatively low-resolution adrenal images. The introduction of a pinhole collimator for adrenal scintigraphy in 1975[21] has enabled us to obtain the high-resolution adrenal images. In Part I, the analysis of normal adrenal diverging and pinhole images with ^{131}I-Adosterol was performed and the important points on interpretation of the adrenal images were discussed according to its results[22].

In this paper, analysis of the adrenal images with ^{131}I-Adosterol is made in patients with various adrenal diseases such as aldosteronism, Cushing's syndrome, pheochromocytoma, adrenogenital syndrome, metastatic tumors etc. and in the adrenal adjacent or gonadal hormone-producing tumors, to establish the adrenal imaging patterns. The diagnostic accuracies depening upon these imaging findings and the adrenal high/low ratios are also studied. In some patients, the tissue concentrations and other data of the removed specimens are estimated.

Materials and Methods

Table 1 shows a list of 48 selected cases which were presented from Feb. 1975 to July 1980. Of these cases, 28 (14; primary aldosteronism, 6; Cushing's syndrome, 3; pheochromocytoma, 1; adrenal cyst, 2; adrenal adjacent tumor, 1; arrhenoblastoma, 1; metastatic tumor) had had operations or an autopsy and their

Table 1. Clinical material

Final diagnosis	No. of cases
Primary aldosteronism	17
Idiopathic aldosteronism	1
Cushing's syndrome	7
Adrenogenital syndrome	2
Pheochromocytoma	3
Nonfunctioning adrenal adenoma	1
Metastatic adrenal tumor	3
Adrenal cyst	1
Bartter's syndrome	2
Adrenocortical insufficiency	6
Adrenal adjacent tumor	4
Arrhenoblastoma of the ovary	1
Total	48

pathological diagnoses had been made. The final diagnoses of the remaining 20 cases were made clinically by routine hormonal assays, adrenal venous hormones measurements, angiography and/or computed tomography.

The details concerning the adrenal imaging technique, computer displays and the calculating methods of the adrenal high/low ratios have been reported in Part I[22]. The essentials of imaging technique are as follows: The imaging is performed 5-9 days after intravenous injection of ^{131}I-Adosterol (about 16 μCi/kg of body weight, made by Daiichi Radioisotopes LTD.) to determine the adrenal location by using a diverging collimator. Each adrenal image is then separately obtained on Polaroid film with the use of a pinhole collimator, which is closely applied to the marked point on the patient's back in a prone position (Pinhole method). The radioactive comparative diagnosis is made on the posterior diverging image obtained 12-14 days postinjection (Diverging method). The scintigraphic estimation of the adenoma size is made by the previously reported method[21].

The tissue concentrations of the tumor and its adjacent adrenal tissue of the removed specimen were counted respectively by a well type scintillation counter. The T./Adj. ratio was calculated as follows; Counts of tumor/g-background counts/ Counts of adjacent tissue/g-background counts. The radioactivities of the removed specimen and the standard source were obtained with the use of a stand type scintillation counter. The adrenal uptake ratio was calculated as follows; (Counts of the removed specimen-background counts/ Counts of the administered dose-background counts)×100%. The radioactivity of the tumor or the adjacent tissue is expressed as the percent of the total dose administered per gram of tissue (% dose/g). It was calculated from the value of the T./Adj. ratio, the adrenal uptake ratio and the weights of the tumor and the adjacent tissue.

Results

I. Imaging pattern analysis and diagnostic accuracy

1) Aldosteronism

Table 2 shows the results of aldosteronism. Visualization of both glands was observed on the diverging images of this group. In 18 patients with aldosteronism, 10 showed "lateralization". This meant that radioactivity of the tumor-bearing gland was definitely higher than that of the contralateral gland (Fig. 1A and 2A). 4 patients showed slightly asymmetrical uptakes which could not be differentiated from normal asymmetry (fig. 3A). 3 patients showed symmetrical uptakes on their diverging images (Fig. 4A). In one patient with idiopathic aldosteronism (hyperplasia), the left gland was slightly higher in radioactivity than the right gland on the diverging image (Fig. 5A). Depending upon the criterion of "lateralization", the diagnostic accuracy in locating the tumor-bearing gland in primary aldosteronism (aldosteronoma) was 59% (10/17). The size of the largest adenoma with a slightly asymmetrical uptake was 1.5×1.3×1.0 (=1.95) cm^3. The smallest adenoma with "lateralization" and the next to the smallest adenoma were 1.4×1.4×0.6 (=1.12) cm^3, and 1.6×1.5×1.0 (=2.4) cm^3 in size respectively. "Lateralization" may almost always be produced when the adenoma is greater than 2.0 cm^3, when multiplying the three dimentional diameters.

The basic pattern of the original pinhole image in primary aldosteronism is that an adenoma is visualized as a hot nodule (round high-radioactive area) and its ipsilateral adjacent adrenal tissue and the contralateral gland are also visualized. In other words, it is a hot nodule added to either of both normal pinhole imaging types (Fig. 1-4). The adenoma is represented as a peak-formation on the 90°-rotated 3 dementional display (Fig. 1 and 4). In 15 of the 16 patients (94%) with primary aldosteronism whose pinhole images were obtained, the adenoma could be located correctly by the baseline pinhole images. In one patient whose baseline pinhole images showed three high-radioactive areas (one on the left image and two on the right image), the adenoma at the inferior portion of the right gland was detected as a hot nodule on the suppression pinhole image. In one

Table 2. Results of aldosteronism

Case	Age	Sex	Diverging image	Pinhole image		Final diagnosis	
			Lateralization	Portion of a hot nodule	Size (cm)	Affected side	Size (cm)
1. T.H.	42	♀	L	—	—	L	1.6×1.5×1.5
2. M.Y.	30	♂	?	L-inferior	1.3×1.1	L	1.3×1.3×0.9
3. E.I.	46	♀	R(?)	R-middle	1.4×1.1	°R	1.5×1.3×1.0
4. T.M.	41	♀	R	R-middle	2.1×1.5	R	2.0×1.7×1.2
5. K.S.	35	♀	L	L-inferior	1.2×1.2	L	1.4×1.4×0.6
6. H.K.	42	♀	R(?)	R-inferior*	1.2×1.2*	R	1.4×1.3×0.9
7. K.N.	40	♀	L	L-superior	2.1×2.0	L	2.2×2.0×1.7
8. E.A.	43	♀	R	R-superior	1.5×1.3	R	1.6×1.5×1.0
9. K.U.	43	♀	L	L-superior	1.6×1.5	L	1.7×1.6×1.0
10. T.D.	36	♂	R(?)	R-inferior	1.3×1.3	R	1.9×1.8**
11. E.K.	43	♀	?	L-superior	1.5×1.2	L	1.5×1.1***
12. H.S.	50	♀	R	R-inferior	2.8×2.6	R	2.8×2.8×1.9
13. H.K.	54	♀	R(?)	R-superior	0.9×0.8	R	1.0×1.1***
14. F.G.	54	♀	?	L-superior	1.2×0.8	L	1.2×0.9×0.9
15. M.S.	61	♂	L	L-inferior	2.7×2.5	L	2.6×2.5×2.0
16. T.Y.	33	♀	L	L-superior	1.7×1.5	L	1.8×1.6×1.2
17. K.H.	40	♂	L	L-mid-lateral	2.0×1.8	°L	2.0×2.0×1.2
18. N.I.	53	♂	L(?)	Both normal types	—	Both	Hyperplasia

*Dexamethasone suppression image, **On angiogram, ***On CT image, °Adenoma with hyperplasia

patient with idiopathic aldosteronism, both glands showed normal pinhole imaging types (Fig. 5). In 16 of the 17 patients with aldosteronism (94%), the correct diagnosis could be made by the baseline pinhole imaging alone. In 13 patients who had adrenal operations, the size of the adenoma and its location on the gland estimated by the pinhole imaging were almost the same as those of the removed specimen. The smallest adenoma (Fig. 4) and the largest adenoma (Fig. 2) in this series were $1.2\times0.9\times0.9\,cm^3$ and $2.8\times2.8\times1.9\,cm^3$ in size respectively.

2) Cushing's syndrome

In 3 patients with cortisol-producing adenomas, the diverging imaging pattern showed unilateral visualization of the tumor-bearing gland. The pinhole image clarified the radiocholesterol uptake of the adenoma alone which was visualized and supported by the findings of the removed specimen (Fig. 6). Therefore, the imaging pattern of the patient with a cortisol-producing adenoma can be described as visualization of the adenoma with nonvisualization of the ipsilateral adjacent adrenal tissue and the contralaterla adrenal gland.

In 2 patients with adrenal hyperplasia, the diverging images showed bilateral visualization and the pinhole images revealed both normal types in one of the patients (Fig. 7). Both swelling triangular appearances were shown in the other patient (Fig. 8). In one patient with recurrent Cushing's syndrome a few years after a left adrenalectomy due to an adenoma, the diverging image showed intense radioactivity of the right gland with lack of the left concentration. A swelling triangular appearance was observed on the right pinhole image which enabled me to differentiate hyperplasia from an adenoma (Fig. 9). In only one patient with a cortisol-producing adrenocortical carcinoma, the right adrenal region alone was visualized on the diverging image. The pinhole image showed a cap-like deposit of the right gland. Comparing the scintigram of the removed

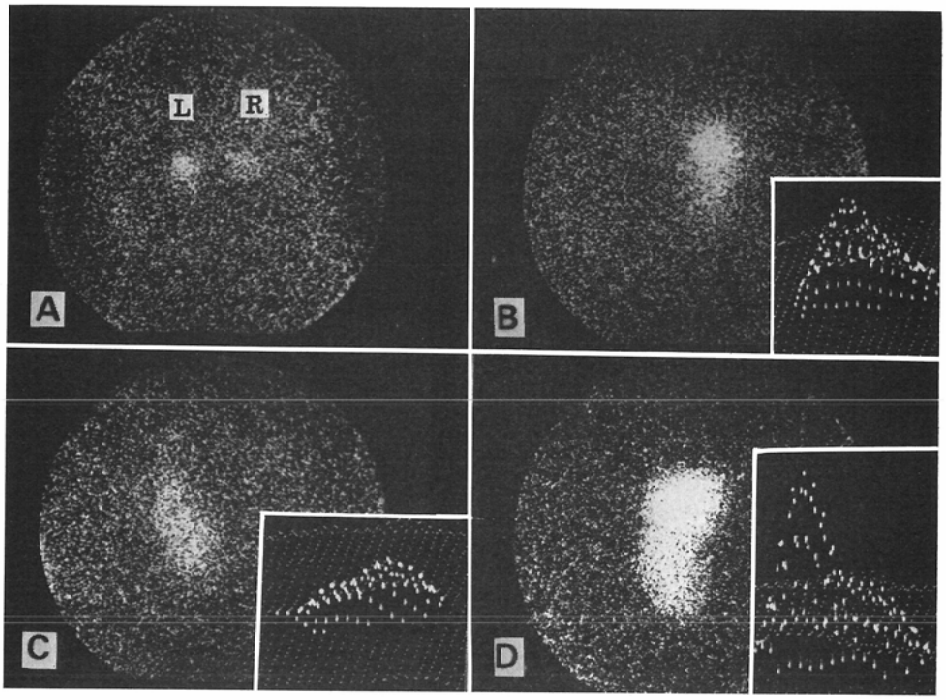

Fig. 1

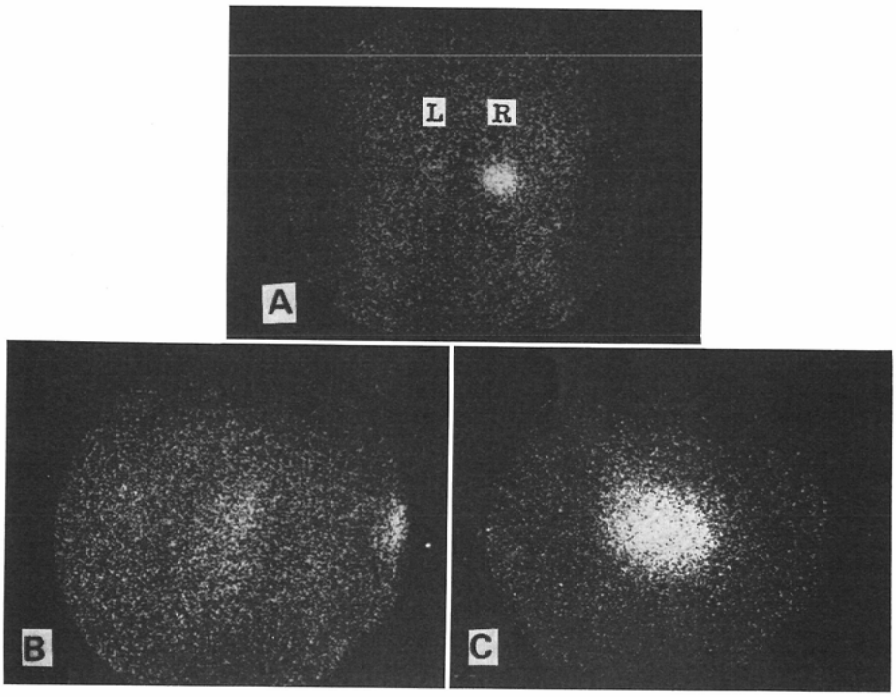

Fig. 2

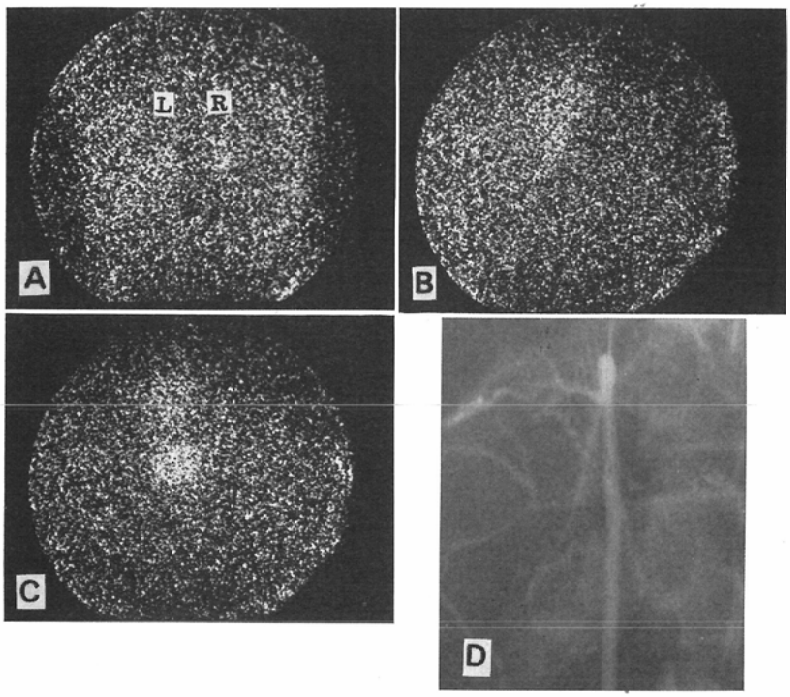

Fig. 3

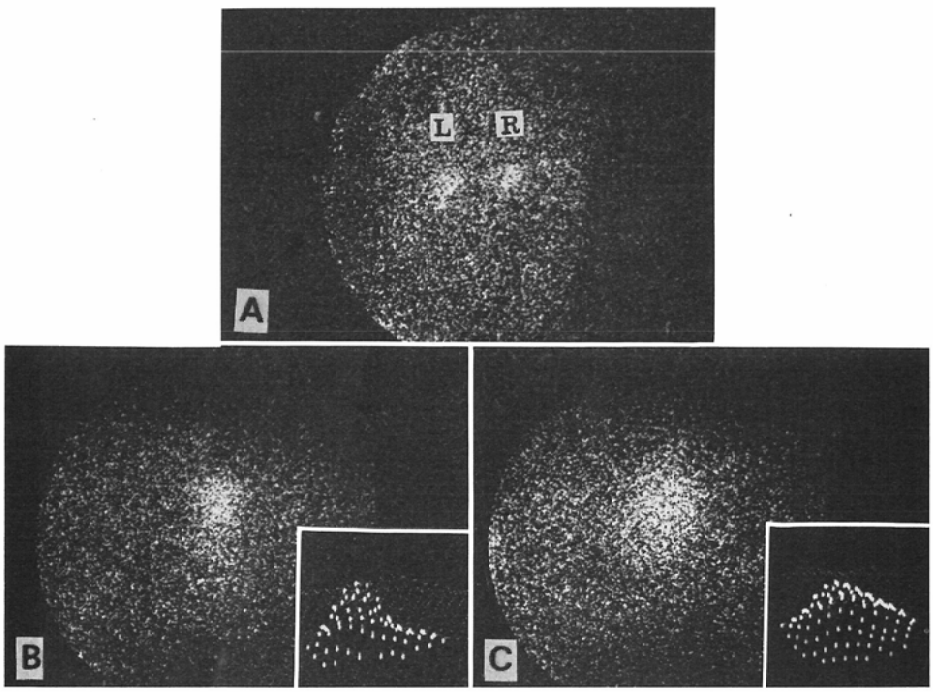

Fig. 4

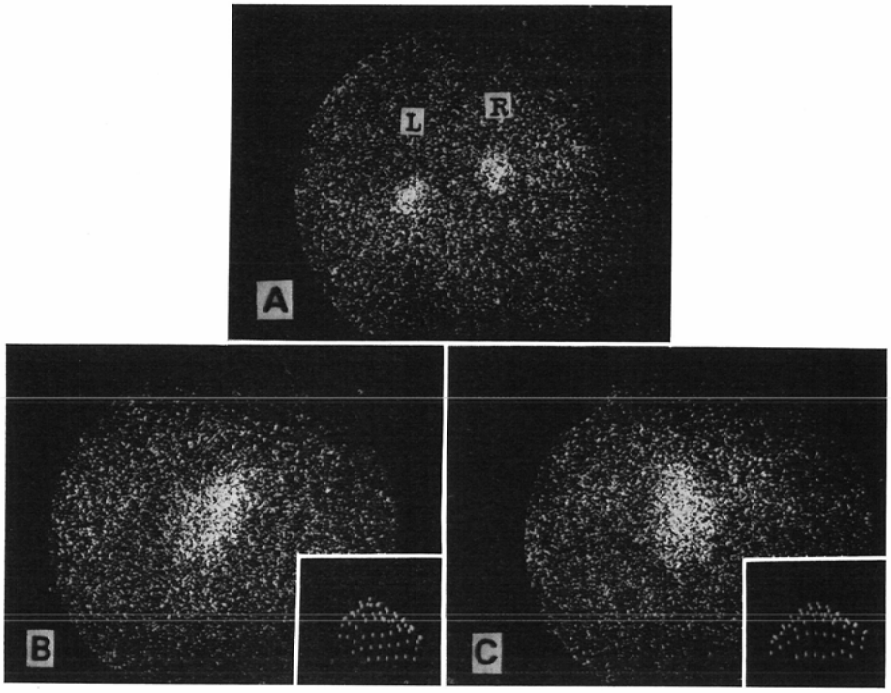

Fig. 5

specimen with its pathological findings proved that the positive part was well differentiated and the negative part was undifferentiated carcinomas respectively[23] (Fig. 10).

3) Adrenogenital syndrome

One patient with congenital adrenal hyperplasia secondary to a C-21 hydroxylase deficiency showed a bilateral asymmetrical uptake on the diverging image and swelling triangular shapes on the pinhole images (Fig. 11). In another patient with a large androgen-producing carcinoma of the left gland, the tumor itself showed diffuse lower radioactivity. The contralateral gland was also visualized as a hot spot on the diverging image which was delineated as a normal triangular type on the pinhole image (Fig. 12).

4) Pheochromocytoma

The diverging image of one patient with a large malignant pheochromocytoma ($8.0\times5.5\times4.0\,cm^3$ in size) showed a complete defect of the tumor-bearing gland (Fig. 13). In the other two patients with relatively small tumors of the right glands, the right glands showed slightly higher asymmetrical uptakes on their diverging images. These two tumors, however, were delineated as defects on the pinhole images (Fig. 14 and 15). A pheochromocytoma, therefore, is shown as a cold area or defect according to its size.

5) Miscellaneous adrenal tumors

A patient with a nonfunctioning adenoma of the right gland showed a right higher asymmetrical uptake on the diverging image and it was delineated as a relatively high-radioactive area on the pinhole image. In three patients with metastatic adrenal tumors from lung cancer and one patient with an adrenal cyst, the tumor-bearing glands showed complete defects or low radioactivity on their diverging images. In two adrenal glands with a metastatic tumor $6.0\times6.5\times7.0\,cm^3$ and a cyst $5.0\times4.0\times4.5\,cm^3$ on their CTs, their pinhole images showed nearly complete defects. One adrenal gland with a metastatic tumor $3.0\times3.0\times3.0\,cm^3$ on its CT showed low rimmed radioactivity surrounding the tumor on the pinhole image (Fig. 16). The smallest metastatic tumor

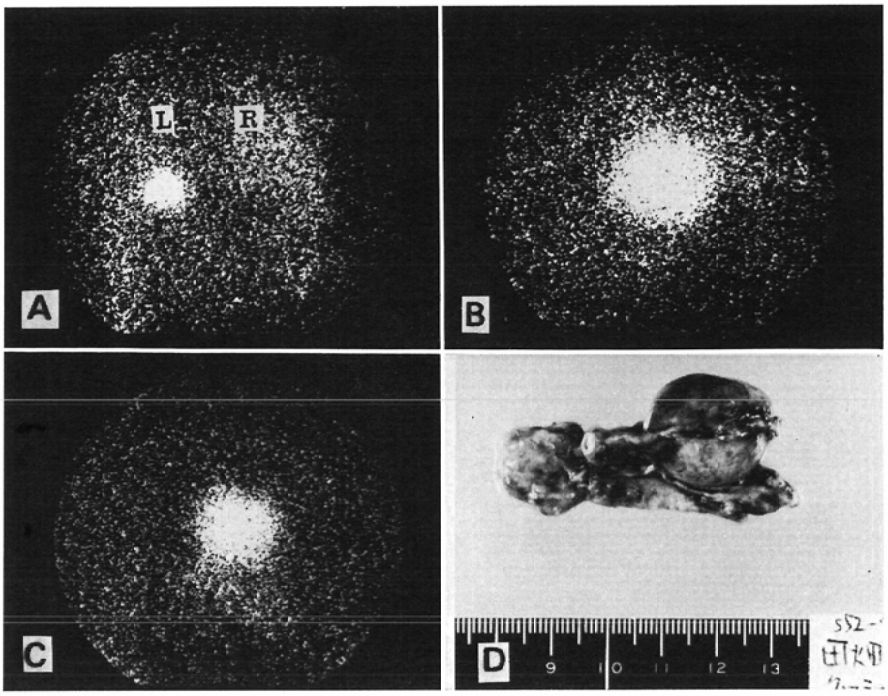

Fig. 6

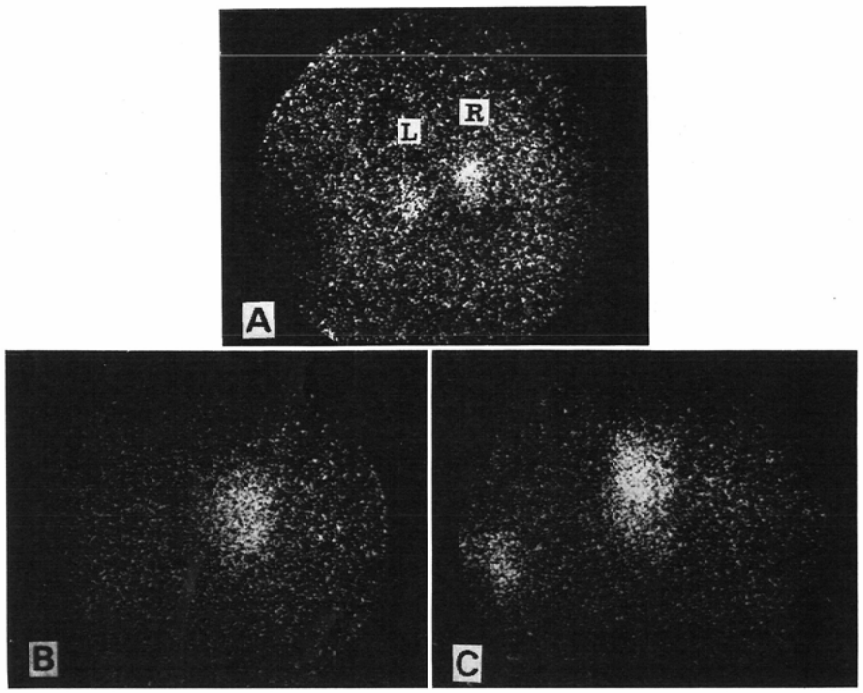

Fig. 7

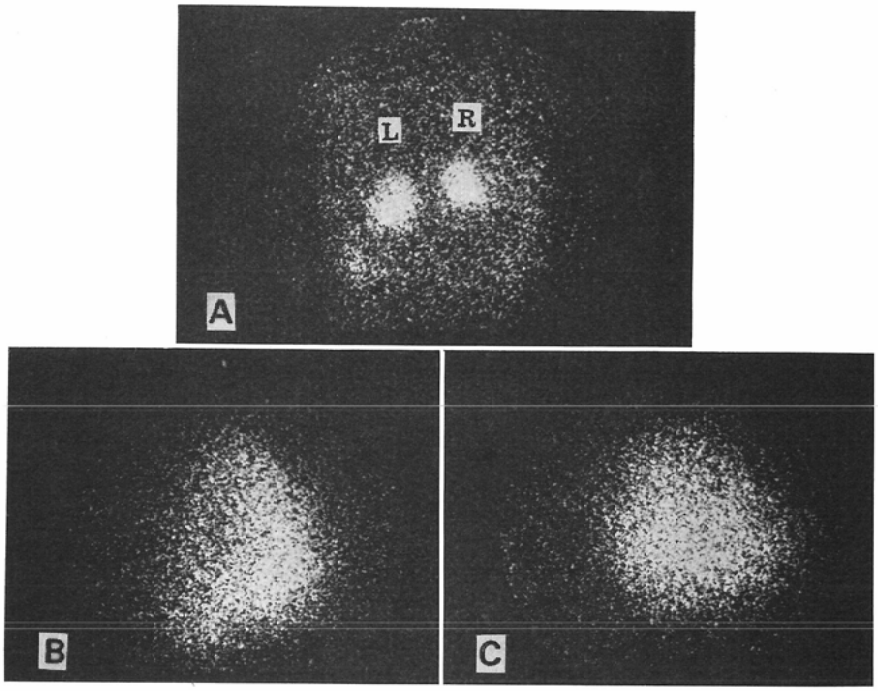

Fig. 8

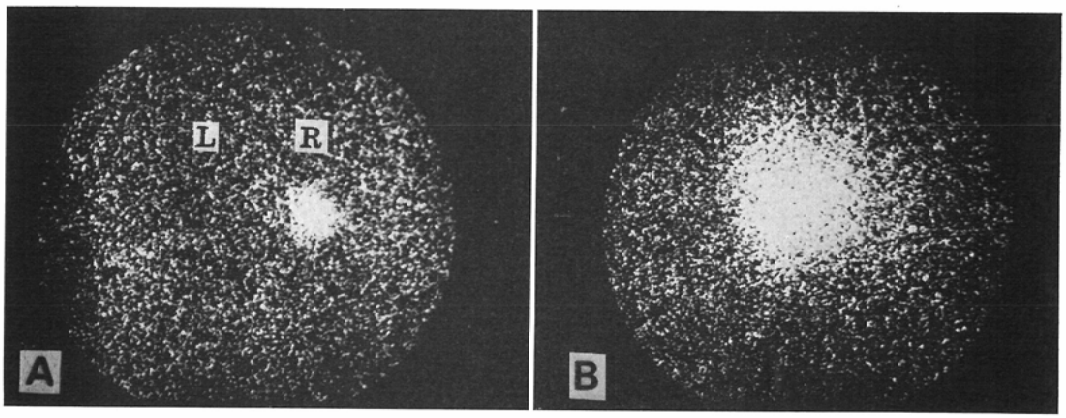

Fig. 9

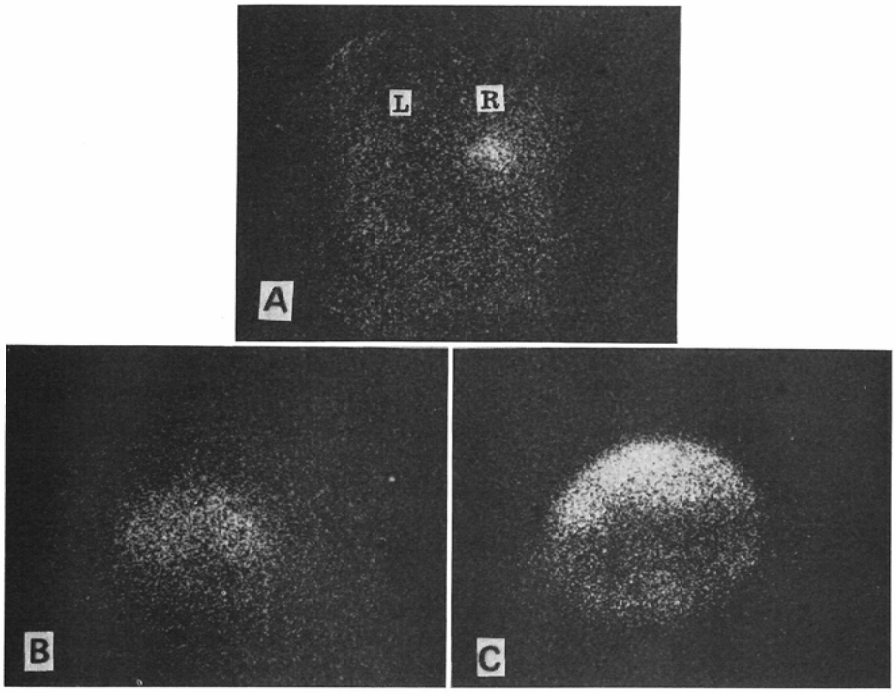

Fig. 10

whose size was 1.5×1.5×1.7 cm^3 on autopsy was represented as having a partial defect at the superior portion of the right gland (Fig. 17).

6) Bartter's syndrome

In two patients with Bartter's syndrome, the right higher asymmetrical uptakes were observed on their diverging images and both glands showed normal adrenal pinhole types (Fig. 18).

7) Adrenocortical insufficiency

In two patients with primary adrenocortical insufficiency and four with secondary adrenocortical insufficiency, bilateral faint visualization or nonvisualization was the diverging imaging pattern (Fig. 19).

8) Adrenal adjacent tumors

The diverging images of 2 patients with splenic cysts and one patient with a left-sided retroperitoneal hematoma showed significant lower localization of the left glands compared to the right glands. This is due to the pressure effect of these masses (Fig. 20). One right renal cyst produced a pressure effect on the right gland and its upward displacement was also recognized (Fig. 21). Two mass lesions (a splenic cyst and a right renal cyst) produced concave pressure effects on the adrenals. The other mass-sided glands showed normal configuration on their pinhole images.

9) Extraadrenal sex hormone-producing tumor

An arrhenoblastoma, an androgen-producing ovarian tumor, was visualized with ^{131}I-Adosterol[24] (Fig. 22). Both adrenals in this patient were visualized and showed normal pinhole imaging types.

10) Summary of adrenal imaging patterns and diagnostic accuracy

Fig. 23 shows the schematic representation of adrenal diverging and pinhole imaging patterns. The diverging images may be divided into seven patterns: I. Bilateral symmetrical or asymmetrical visualization, II.

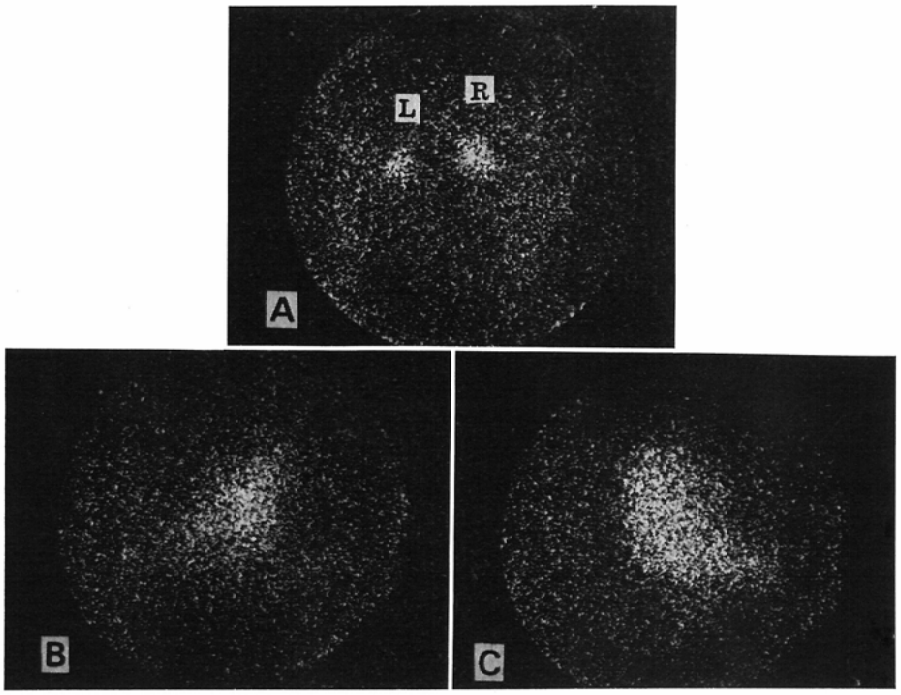

Fig. 11

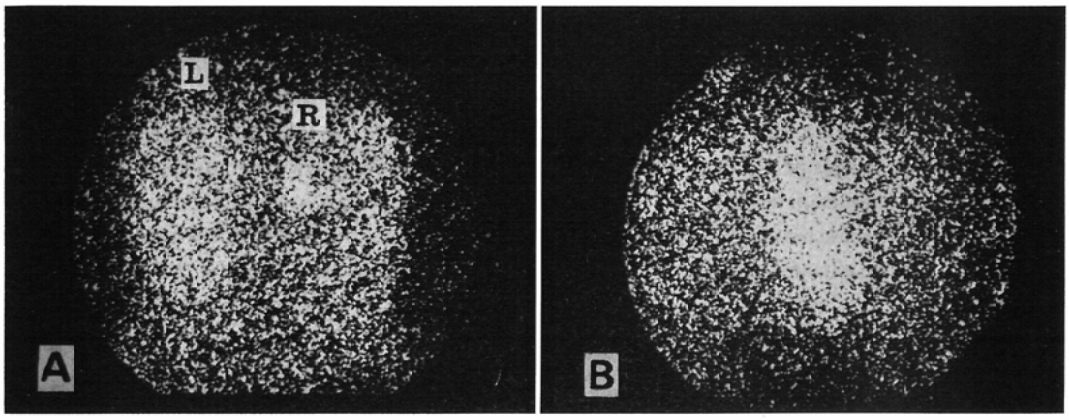

Fig. 12

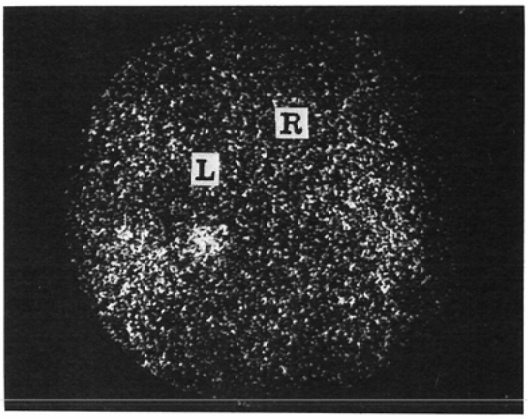

Fig. 13

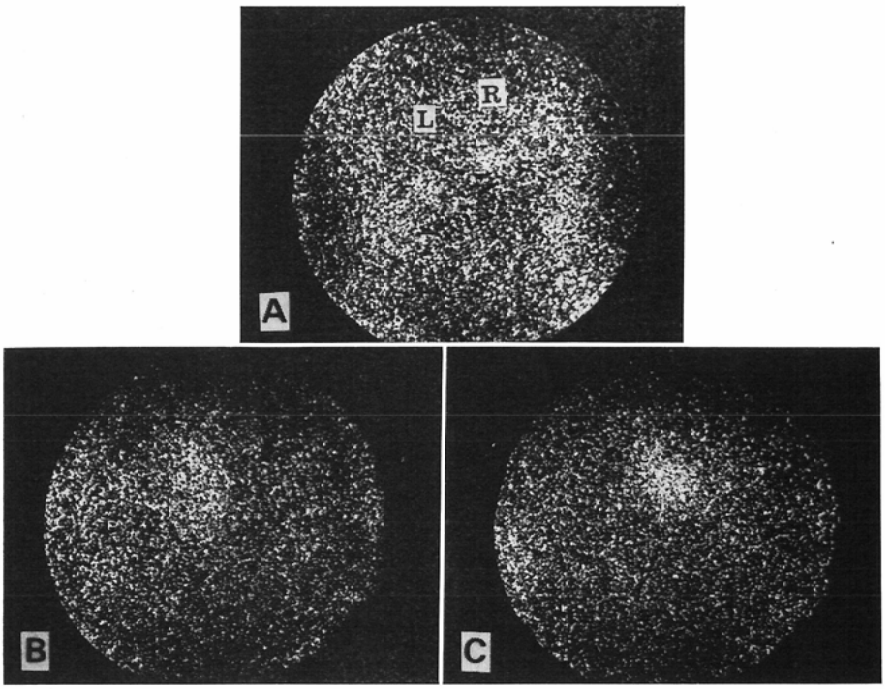

Fig. 14

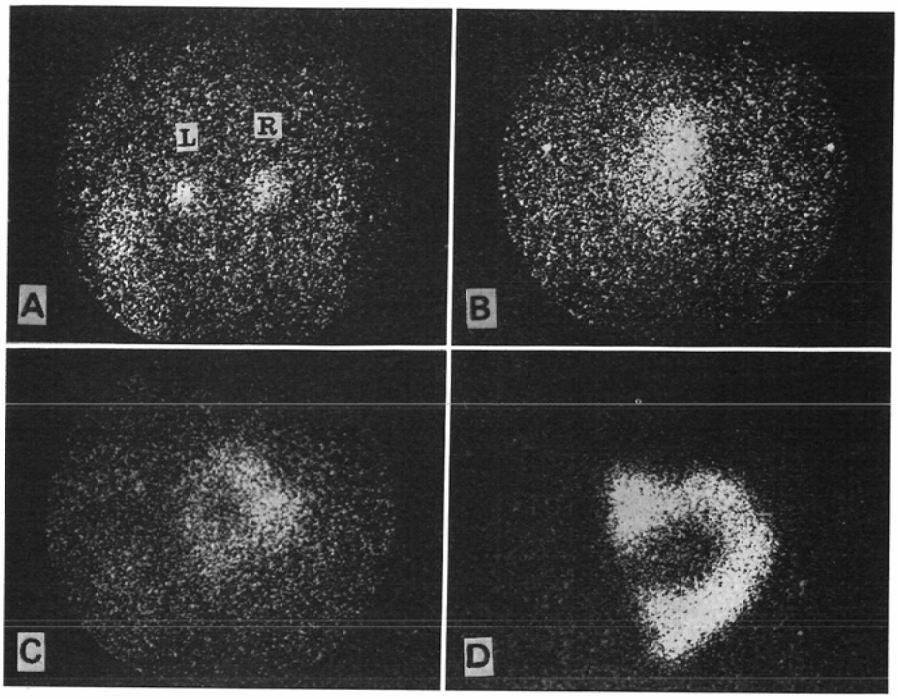

Fig. 15

Unilateral visualization, III. Bilateral faint visualization, IV. Bilateral nonvisualization, V. Location abnormality, VI. Unilateral visualization with contralateral diffuse deposit and VII. Bilateral visualization with extraadrenal deposit. The pinhole images may also be divided into one to several patterns in each diverging pattern: I.A. Bilateral normal adrenal type, B. Unilateral hot nodule added type, C. Bilateral hot nodule added type, D. Unilateral rim-like or partial defect type, E. Bilateral partial defect type, F. Bilateral hot nodule alone type and G. Bilateral swelling type, II.A. Normal type, B. Hot nodule alone type, C. Lower deposit or partial defect type and D. Swelling type, III.A. Normal outline type and B. Indefinite type, IV.A. Bilateral nonvisualization, V.A. Bilateral normal type and B. Unilateral compressed type, VI.A. Diffuse low deposit type with contralateral normality and VII.A. Bilateral normal type with tumor shaped deposit.

The possible lesions or conditions and diseases in this series corresponding to these imaging patterns are summarized in Table 3.

The diagnostic accuracy in locating the tumor-bearing gland in various adrenal tumors was 70% (21/30, 10 of 17 aldosteronomas, 4 cortisol-producing tumors, one androgen-producing tumor, one of 3 pheochromocytomas, one nonfunctioning adenoma and 4 metastatic tumors) with the diverging imaging whose diagnostic criteria depended mainly upon the radioactive comparison between both glands. Diagnostic accuracy was 97% (28/29, 15 of 16 aldosteronomas, 4 cortisol-producing tumors, one androgen-producing tumor, 3 pheochromocytomas, one nonfunctioning adenoma and 4 metastatic tumors) with the pinhole imaging whose diagnostic criteria depended mainly upon the morphological aspects of both glands.

II. Adrenal high/low ratios

The main purpose in obtaining these ratios is their aid in evaluating the adrenal tumor-bearing glands. Fig. 24 shows the result of the adrenal high/low ratios on both views in various adrenal diseases. These are

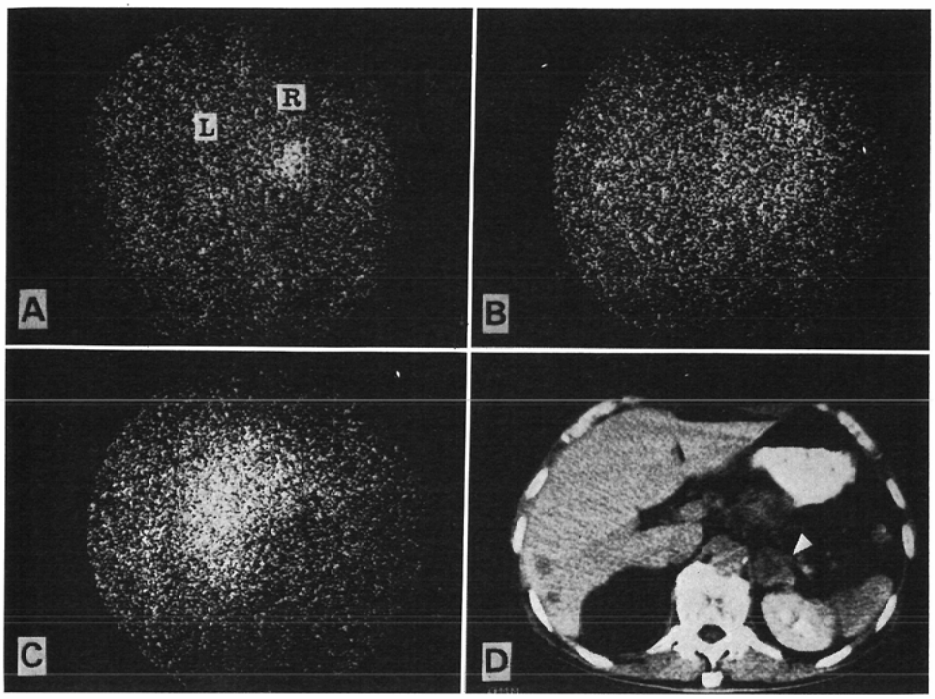

Fig. 16

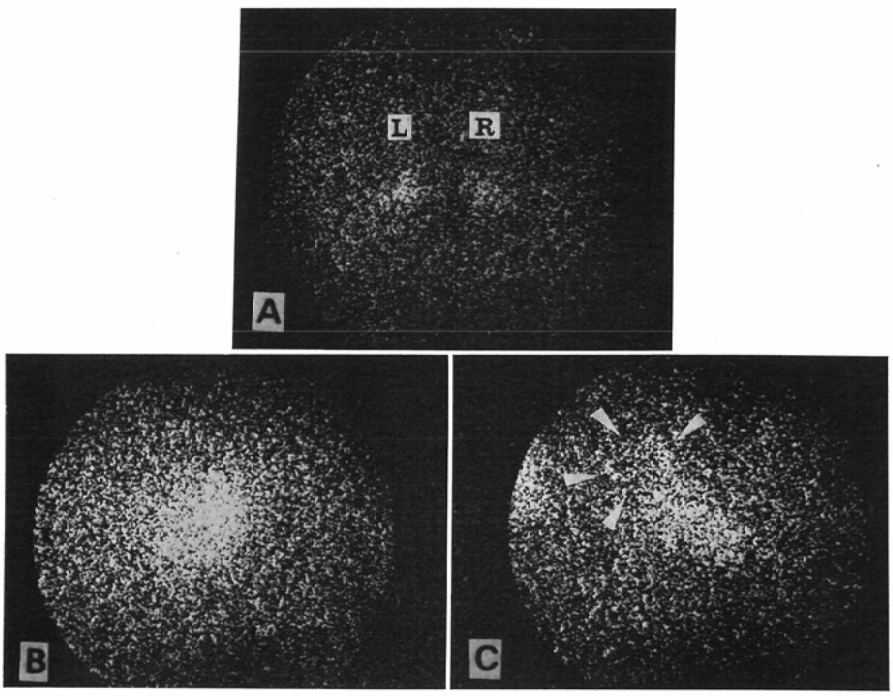

Fig. 17

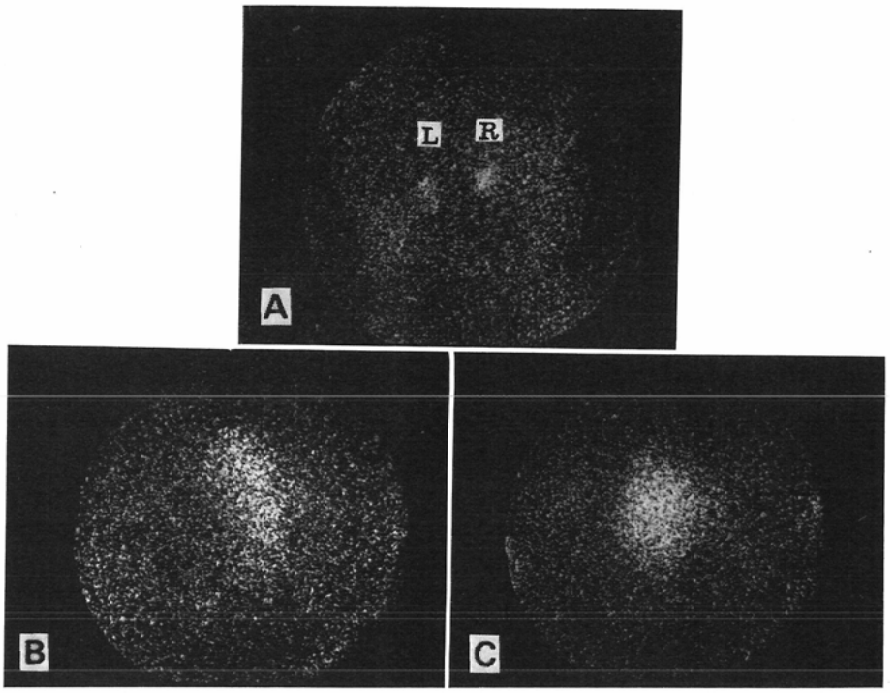

Fig. 18

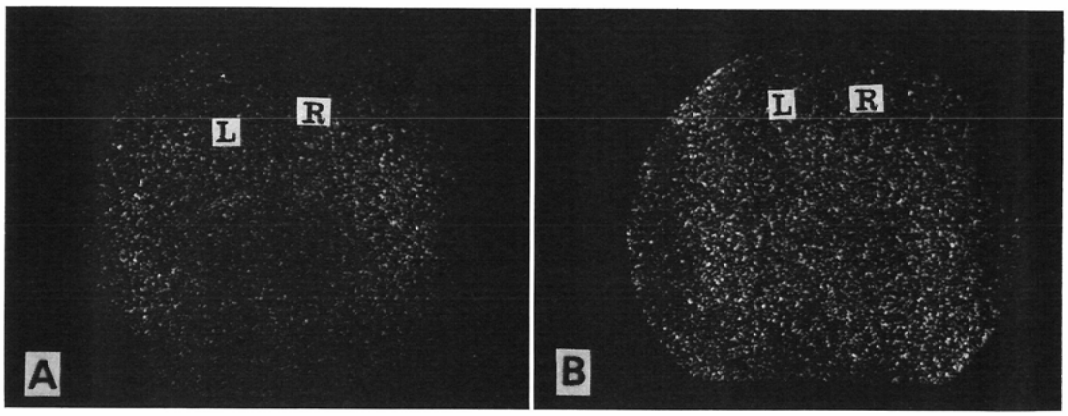

Fig. 19

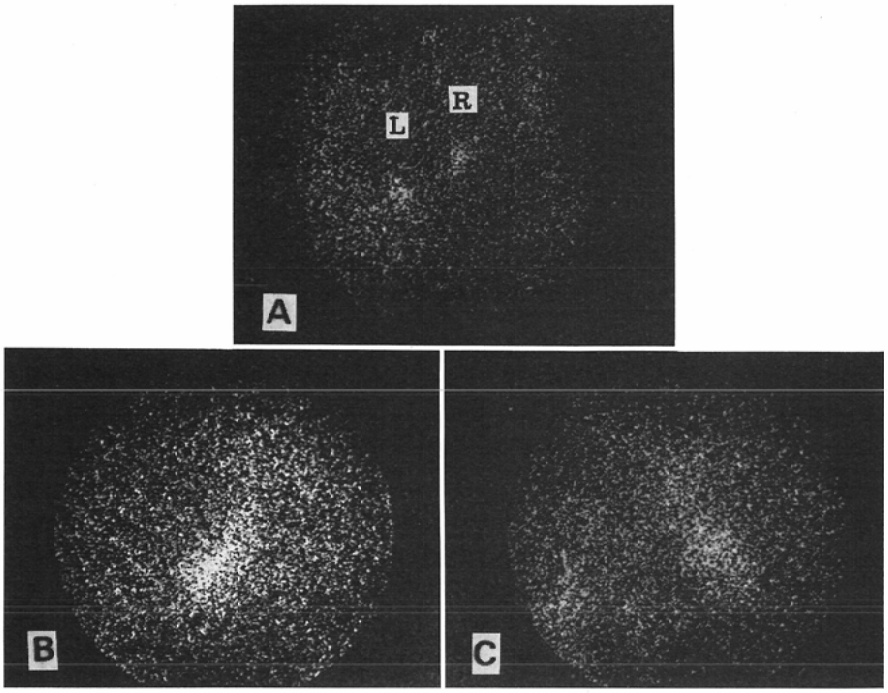

Fig. 20

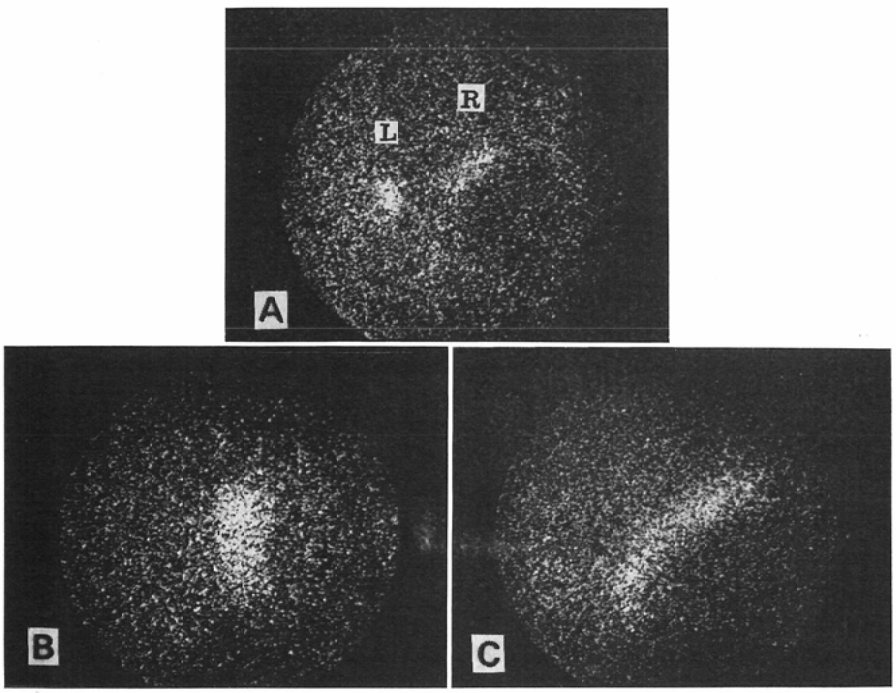

Fig. 21

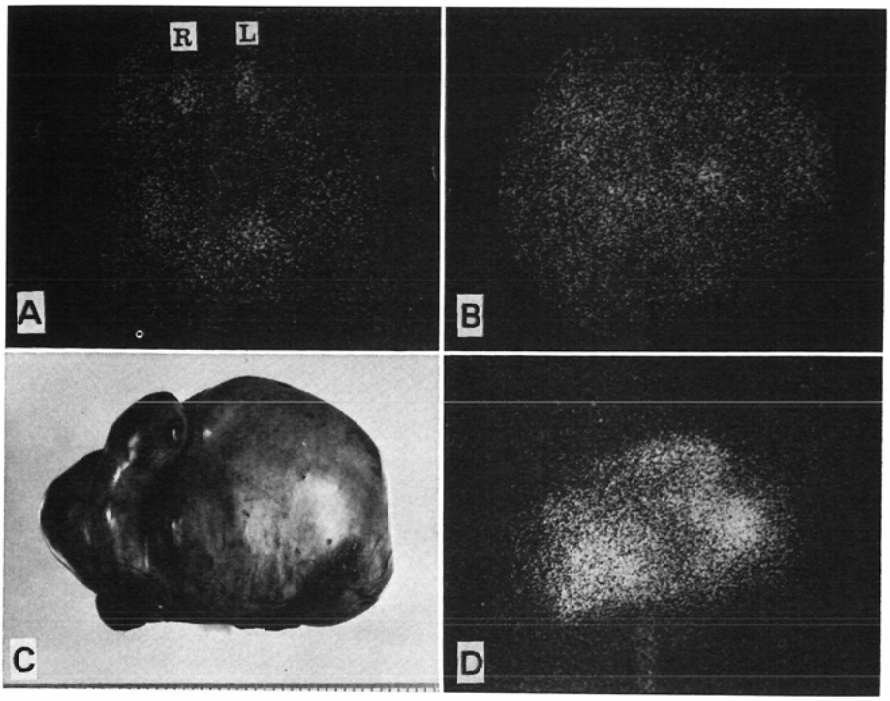

Fig. 22

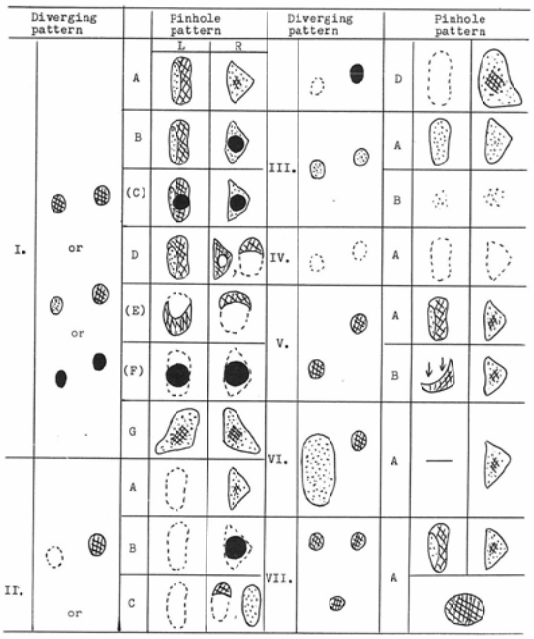

( ); unexperienced, but possible pattern.
Degree of accumulation: ●; marked, #; moderate, ·; slight, ○; negative.

Fig. 23. Schematic representation of the adrenal imaging patterns.
See text. The possible lesions or conditions and diseases in this series corresponding to these imaging patterns are shown in Table 3.

Table 3. Possible lesions or conditions and diseases in this series corresponding to each adrenal imaging pattern

Pattern		Possible lesions or conditions	Diseases in this series
I.	A	Bilateral normal adrenals Bilateral hyperplasia Lesions not to be detected	Idiopathic aldosteronism Cushing's hyperplasia Bartter's syndrome
	B	Unilateral noncortisol steroid hormone-producing or nonfunctioning adenoma	Primary aldosteronism Nonfunctioning adenoma
	C	Bilateral noncortisol steroid hormone-producing or nonfunctioning adenomas	
	D	Unilateral noncortical tumor or cortex-destroying lesion	Pheochromocytoma and metastatic cancer
	E	Bilateral noncortical tumors or cortex-destroying lesions	
	F	Bilateral cortisol-producing adenomas	
	G	Bilateral hyperplasia	Cushing's hyperplasia and AGS due to hyperplasia
II.	A	Unilateral total adrenalectomy Unilateral noncortical tumor or cortex-destroying lesion	Pheochromocytoma, adrenal cyst and metastatic cancer
	B	Unilateral cortisol-producing adenoma	Cushing's adenoma
	C	Unilateral cortisol-producing carcinoma Bilateral noncortical tumors or cortex-destroying lesions	Cushing's carcinoma
	D	Unilateral hyperplasia after contralateral total adrenalectomy	Cushing's hyperplasia
III.	A,B	Bilateral cortical atrophy Bilateral noncortical tumors or cortex-destroying lesions Administration of the inappropriate tracer, inappropriate dose of the tracer or corticosteroid Hyperlipidemia	Adrenocortical insufficiency
IV.	A	The same lesions or conditions as III Unilateral cortisol-producing carcinoma	Adrenocortical insufficiency
V.	A,B	Pressure effect due to an adrenal adjacent tumor	Splenic or renal cyst and retroperitoneal hematoma
VI.	A	Unilateral sex hormone-producing carcinoma	AGS due to carcinoma
VII.	A	Sex hormone-producing gonadal tumor	Arrhenoblastoma of the ovary

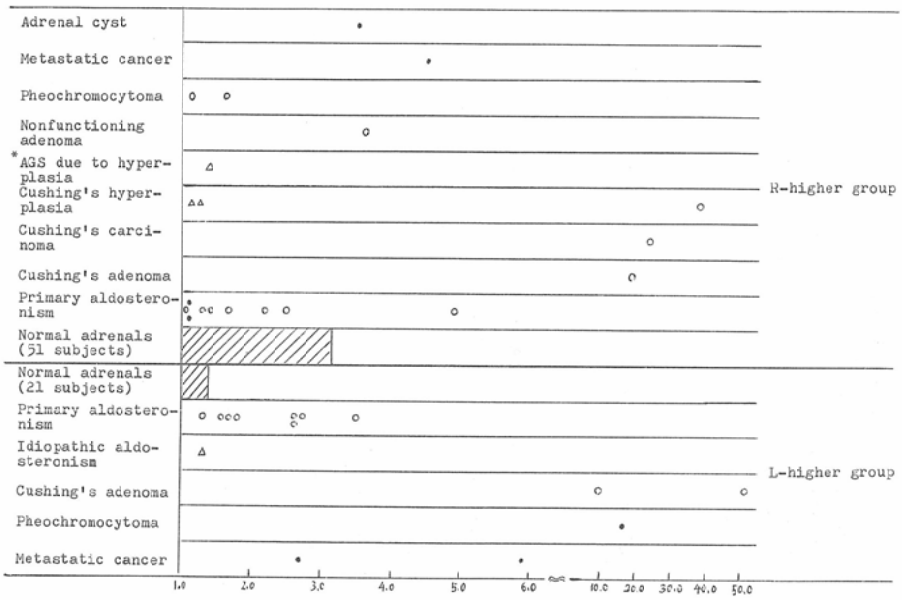

o; higher side = affected gland, •; lower side = affected gland, △; both hyperplasia

* Adrenogenital syndrome

Fig. 24. Result of adrenal high/low ratios on both views.

considered to be approximate to the true high/low ratios[22]. In 17 patients with primary aldosteronism, the ratios ranged from 1.06 to 4.81 and the tumor-bearing glands were the higher sides in 15 of these patients (88%). In 2 patients with left-sided adenomas whose sizes were 1.2×0.9×0.9 cm^3 on the removed specimen and 1.5×1.1 cm^2 on the CT respectively, the left glands were the lower sides.

3 patients with Cushing's adenomas and one with Cushing's carcinoma had ratios which were very high. One nonfunctioning adenoma-bearing gland was the higher side and its ratio was 3.60. In 2 of the 3 patients with pheochromocytomas, the tumor-bearing glands were the higher sides, although the tumors themselves were represented as defects or cold areas on their pinhole images. All 4 metastatic tumor-bearing glands were the lower sides. In 25 of the 29 patients (86%) with adrenal tumors, the higher or lower sides were reasonable. In 4 patients with bilateral adrenal hyperplasia, high/low ratios ranged from 1.15 to 1.38 and 3 of them showed the right higher ratios.

The normal adrenal high/low ratios ranged from 1.01 to 3.15 in the right higher group and from 1.01 to 1.41 in the left higher group[22]. Only 6 of the 16 patients (38%) with adrenal tumors in the right higher group and 12 of the 13 patients (92%) with adrenal tumors in the left higher group had ratios above the normal highest ratios. In primary aldosteronism, the ratio above the normal highest ratio was observed in only one of the 9 right higher ratios. However, ratios above the normal highest ratio were observed in 7 of the 8 left higher ratios.

These results suggest that the left higher ratios (≧1.5 in this study) have high diagnostic value in locating the tumor-bearing glands because of the high discrepancy between normal and abnormal ratios, and the right higher ratios are less diagnostic because of the high overlap between them.

Concerning the ratios on each view, the higher or lower sides were reasonable in 26 of the 29 patients with adrenal tumors (90%) on the posterior view and in 25 of them (86%) on the anterior view. 6 of the 15 patients with adrenal tumors (one of 8 patients with aldosteronomas) in the right higher group and 9 of the 14 patients

with adrenal tumors (4 of 9 patients with aldosteronomas) in the left higher group showed ratios above the normal highest ratios (r:3.47, 1:1.64)[22] on the posterior view. On the anterior view, 6 of the 16 patients with adrenal tumors (2 of 9 patients with aldosteronomas) in the right higher group and 8 of the 13 patients with adrenal tumors (5 of 8 patients with aldosteronomas) in the left higher group showed ratios above the normal highest ratios (r:2.73, 1:2.54)[22].

III. Tissue concentration

Table 4. Summary of various data from the removed specimens

Disease	Patient	Adrenal uptake ratio (%)	Weight		T/Adj. ratio	% dose/g		Dose* (mCi)	Interval** (days)
			Tumor	Adj. tissue		Tumor	Adj. tissue		
Primary aldosteronism	1. K.S.	0.63	1.04	3.66	2.8	0.27	0.097	0.95	7
	2. K.N.	0.89	4.0	8.0	2.1	0.11	0.053	0.92	7
	3. E.A.	0.77	2.0	4.5	1.8	0.17	0.093	1.0	9
	4. K.U.	0.64	2.3	3.6	1.4	0.13	0.092	0.4	6
	5. H.S.	1.38	8.0	5.0	1.7	0.13	0.074	1.0	5
	6. T.Y.	0.60	2.2	3.5	4.0	0.20	0.050	1.0	7
	7. M.Y.	—	—	—	4.3	—	—	0.8	7
	8. T.M.	—	—	—	1.6	—	—	0.8	7
	9. H.K.	—	—	—	1.0	—	—	1.0	4
	10. F.G.	—	—	—	0.41	—	—	0.7	4
	11. M.S.	—	6.5	1.5	12.0	—	—	0.98	35
Cushing's adenoma	12. T.N.	5.2	3.2	1.9	6.4	1.49	0.23	0.47	5
Cushing's carcinoma	13. F.I.	0.88	120	—	—	0.0073	—	1.0	2
Pheochromocytoma	14. T.U.	0.55	—	—	0.031	—	—	1.2	2
	15. M.A.	0.14	20	4.0	0.039	0.0011	0.029	0.85	5

*Administered dose, **Interval between tracer injection and operation

Table 4 shows the summary of various data from the removed specimens. Some of these patients had been given dexamethasone or ACTH, however their administration had ceased at least 11 days before the tracer injection was given. The influence of these exogenous hormones was negligible. In 6 cases of primary aldosteronism, the adrenal uptake ratios ranged from 0.60 to 1.38% with an average of 0.82%. The T./Adj. ratios in 11 cases of primary aldosteronism showed high variation, ranging from 0.41 to 12.0 (median: 1.8, avarage: 3.01), however 6 of these values ranged from 1.0 to 2.1 and 3 of these values ranged from 2.8 to 4.3. Percent dose/g ranged from 0.11 to 0.27% (mean: 0.17±0.06) in 6 aldosteronomas and from 0.05 to 0.097% (mean: 0.077±0.02) in their adjacent adrenal tissue. A Cushing's adenoma showed a high adrenal uptake ratio (5.2%) and percent dose/g (1.49%), whereas a Cushing's carcinoma showed a lower uptake ratio (0.88%) and percent dose/g (0.0073%). The T./Adj. ratios of the two benign pheochromocytomas were 0.031 and 0.039 respectively.

Discussion

In many institutes, adrenal imaging has been performed using a scanner or a gamma camera with a multiparallel collimator. These instruments as well as a gamma camera with a diverging collimator provide an image resolution which is insufficient for outlining the shape of the adrenal gland or the adrenal tumor[5)14)]. The scintigraphic diagnosis by these images has been obtained mainly by the comparison of radioactivity between both glands or the degree of concentration of the tracer in the adrenals. The pinhole images reported previously[21)] and in this series have higher resolution and are equal in morphological aspects to the findings of adrenal venography, especially in the tracer accumulating adrenal lesion (see Fig. 3). These pinhole images enabled me to precisely analize the adrenal images in various adrenal diseases or conditions, following the assessment of both adrenal radioactivities and the location of both glands by the diverging images. The reasons that a pinhole collimator has not been used in other institutes have already been discussed in Part I[22)].

The baseline imaging finding of primary aldosteronism reported previously was both adrenal visualization which showed an asymmetrical or symmetrical uptake and the tumor-bearing gland showed increased radioactivity in general[10)]. With the pinhole images in this study, an adenoma was visualized as a hot nodule and the ipsilateral adjacent adrenal tissue and the contralateral gland were also visualized. This imaging pattern can be explained by the fact that aldosterone does not suppress ACTH. The usual diagnostic criterion of diagnosing the aldosteronoma-bearing gland is lateralization of the radioactivity in one gland. With this, the accuracy in diagnosing the tumor-bearing gland was reported to be 81% (17/21) by Seabold et al.[10)] and 70% (9/13) by Fukuchi et al.[9)] in the baseline imaging with ^{131}I-19-iodocholesterol. 7 of the 8 negative adenomas in these reports were located in the left adrenal glands. Their sizes were 0.7, 0.9, 1.1, 1.6 cm in the former and 1.0×1.1×0.9, 1.0×0.8×0.7 (right), 1.5×1.3×0.3, 0.8×0.7×0.8 cm^3 in the latter respectively. The right adenomas whose sizes were 0.6, 0.8, 1.1 cm were lateralized. In this series using ^{131}I-Adosterol, "lateralization" was shown in 59% (10/17). If the slightly asymmetrical cases are included, the accuracy in diagnosing the affected gland increases to 82% (14/17). The three adenomas whose images showed symmetrical uptakes were all located in the left glands, whereas the four adenomas whose images showed slightly higher right asymmetry were all in the right glands. These results suggest that the judgement of lateralization may depend not only upon the tumor size but also upon normal asymmetry, which means that most normal subjects have right higher asymmetrical uptakes on the posterior views[22)]. According to the data, using ^{131}I-19-iodocholesterol[10)], the clear lateralization which does not depend upon the tumor-bearing gland, the normal asymmetry or the subjective judgment may be produced when the tumor size is above 1.6 cm in diameter. In this particular study using ^{131}I-Adosterol, the tumor size which produces clear lateralization may be above 2.0 cm^3 in the product of its three dimentional diameters. The accuracy in the prediction of an adrenal lesion (tumor vs hyperplasia) was 67% (18/27) with ^{131}I-19-iodocholesterol[10)] and 56% (10/18) in this series. These diagnostic limitations might lead to the use of dexamethasone suppression imaging as a first choice in aldosteronism[5)10)17)]. However, with the baseline pinhole imaging, the locating accuracy which includes not only the affected galnd, but also the position and the size of the adenoma was 94% (15/16) and the capability to differentiate an adenoma from hyperplasia was also 94% (16/17), although there was only one patient with hyperplasia. These values are equal or superior to those of dexamethasone suppression imaging with ^{131}I-NP-59[17)]. The detectability of an adenoma with the Pinhole method depends upon the separability of the radioactivities between the adenoma and its adjacent adrenal tissue. This is influenced by the size of the adenoma, its position, the thickness of the adjacent tissue and the T./Adj. ratio. The correct localization of the smallest adenoma 1.2×0.9×0.9 cm^3 in this series in spite of its T./Adj. ratio (0.41) and the experimental results reported previously[21)] promise the detection of an adenoma less than 1 cm in diameter with this Pinhole method. On practical interpretation, the

important points in differentiating the high-radioactive area produced by an adenoma, from the normal or hyperplasia area, are the presence of its roundness and the appreciation of the normal pinhole imaging pattern. If the origin of a high-radioactive area cannot be decided even with these points, dexamethasone suppression imaging will be indicated.

In Cushing's syndrome, three basic patterns were reported[6)18)]: The imaging pattern of hyperplasia showed symmetrical or asymmetrical visualization, that of an adenoma showed unilateral visualization and that of a carcinoma showed bilateral nonvisualization. These imaging patterns can be explained by the level of ACTH and the degree of tracer uptake by the adrenal tumor. The ACTH excess may promote the tracer uptake of both glands. The high accumulation of the tracer in the adenoma and ACTH suppression secondary to its automonous secretion of cortisol result in unilateral visualization. The carcinoma which accumulates the tracer to a markedly lesser degree per gram and ACTH suppression, result in bilateral nonvisualization. In this study, the diverging images of two patients with hyperplasia and three patients with adenomas agreed with the basic patterns and the pinhole images produced more detailed morphological information. The patient with recurrent Cushing's syndrome after a unilateral adrenalectomy showed unilateral visualization as a matter of course and the important point in this case was that the cause of the unilateral high spot could be detected as hyperplasia by its pinhole image. This could not be done by its diverging image. A pattern differing from the basic pattern was observed in a patient with Cushing's carcinoma. The accumulation of the tracer in the well differentiated carcinomatous part of the tumor resulted in unilateral visualization. Visualization of Cushing's carcinoma and/or its metastases with radioiodocholesterols was also reported by other authors[19)26)-28)]. The tracer uptake of the tumor may depend upon the degree of differentiation of the neoplastic cells. Also, bilateral nonvisualization was observed in a patient with Cushing's hyperplasia and severe hyperlipidemia[29)]. Unilateral visualization alone cannot differentiate an adenoma from a carcinoma and bilateral nonvisualization is not always the indicator of a carcinoma in Cushing's syndrome.

In adrenogenital syndrome, the imaging findings of congenital hyperplasia with ACTH excess may be similar to those in Cushing's hyperplasia as is the case in this paper[9)11)]. The androgen-producing adenoma which I did not experience may produce the same imaging pattern as that of the aldosteronoma. Scintigrams of the patients with androgen-producing adenomas were demonstrated in papers reported by other authors[12)18)]. The androgen-producing carcinoma in this study was shown as a diffuse low-radioactive area with contralateral adrenal visualization. This pattern is different from that of Cushing's carcinoma.

In pheochromocytomas, imaging patterns, total or partial defects according to their sizes were apparent. These results are similar to the results of ^{131}I-19-iodocholesterol[7)], although the adrenal medulla as well as its cortex was reported to greatly uptake ^{131}I-NP-59 in animal study[3)]. The T./Adj. ratios of two benign tumors in this study supported their imaging findings. The simple radioactive comparison between both glands to decide the affected gland is dangerous because the tumor-bearing glands showed higher radioactivity than the contralateral glands in two patients with small tumors. With the Pinhole method, the detectability of the tumor depends not only upon the tumor size but also its location and the presence of rim cortical radioactivity. The centrally located small tumor (Fig. 15) is more detectable than the larger one at the periphery (Fig. 14). Radiopharmaceuticals which concentrate in the adrenal medulla may promise to delineate a pheochromocytoma or neuroblastoma as hot[30)].

The advent of the CT will increase the chances of adrenal imaging in other miscellaneous adrenal tumors[31)]. In fact, the metastatic adrenal tumors, the adrenal cyst and a nonfunctioning adenoma in this study were all pointed out first by the CT. The significance of the adrenal imaging in these tumors may exist in clarifying the relationship between the adrenal cortex and the tumor.

The imaging finding of Bartter's syndrome suggests that secondary aldosteronism produces the same

imaging pattern as a normal subject.

In adrenocortical insufficiency, its imaging pattern was bilateral faint or non-visualization which was the same pattern obtained with ^{131}I-19-iodocholesterol[25].

The abnormal location of the adrenal gland was observed in the patients with adrenal adjacent tumors. In a clinical practice, adrenal imaging can also be used to differentiate whether a retroperitoneal mass lesion originates from the adreanl gland or not.

The possibility and/or success of visualization of the sex hormone-producing gonadal tumors with radioiodinated cholesterols was reported by us[24] and by other authors[32][33] respectively. The mechanism of the tracer accumulation in these tumors is thought to be similar to that in the adrenal cortical tumors. In virilizing or feminizing syndrome, the anterior imaging covering the ovaries or the testes should be done, if the adrenal glands show no abnormality on the adrenal images.

Cholesterol is the principal precursor of the adrenal cortical steroid, concentrates and is stored in the adrenal gland[34]. This is related to the mechanism of concentration of ^{131}I-iodocholesterol in the adrenal gland. From the analysis of the adrenal images with ^{131}I-Adosterol in this series and the review of literature, three principles to make various adrenal images can be induced: 1) Visualization of the cortical tumor depends upon its nature (adenoma or carcinoma), size and the degree of the tracer accumulation in it. 2) The cortisol-producing tumor suppresses tracer accumulation in the ipsilateral adjacent adrenal tissue and the contralateral adrenal gland, whereas the aldosteronoma or androgen-producing adrenal tumor does not suppess it. ACTH excessive condition such as Cushing's disease or adrenogenital syndrome due to congenital adrenal hyperplasia increases the adrenal uptake of the tracer, whereas secondary adrenocortical insufficiency decreases it. These facts indicate that the tracer accumulation in the adrenal gland is related to the level of endogenous ACTH. 3) A noncortical tumor such as a pheochromocytoma, cyst or metastatic tumor produces a cold area or defect according to its size. Other additional factors that influence the adrenal images are: a) Exogenous ACTH or corticosteroid administration, b) Hyperlipidemia, c) Nontumorous adrenal lesions such as inflammation and hemorrhage or extravasation of the contrast media in venography[8], d) Adrenalectomy, e) Administration of the inappropriate tracer or inappropriate dose of the tracer, f) Pressure effect due to the adrenal adjacent tumor and g) Accumulation of the tracer in the sex hormone-producing gonadal tumor. These principles and factors allow summary of the possible lesions or conditions corresponding to each adrenal imaging pattern (Table 3). This summary clarifies that the adrenal imaging patterns are indicative of the possible diseases or conditions, however, in themseleves are nonspecific. Appreciation of these imaging patterns and complete knowledge of the clinical status of the patient is important to make a correct diagnosis.

The results of adrenal high/low ratios, semiquantitative radioactive comparisons between both glands, suggest that they cannot be used as confidential indicators to locate the tumor-bearing glands, especially in primary aldosteronism, although the left higher ratios on both views showed high discrepancy between normal and abnormal subjects. The efforts to obtain the adrenal uptake ratio by external counting methods were made by some authors[6][35]-[37]. Its significance, however, is considered to exist not in locating the tumor-bearing gland or differentiation between an adenoma and hyperplasia in aldosteronism, but in differentiation between normal glands and a hyperfunctioning disease, as Cushing' syndrome.

One of the merits of ^{131}I-Adosterol or ^{131}I-NP-59 compared to ^{131}I-19-iodocholesterol was reported to be earlier visualization of the adrenals[16][17]. The rat adrenal uptakes of the former were reported to be 5 (1 day) and 3 (5 days)[3], 18 (1 day) and 27 (7 days)[38] and 10 (1, 3 and 7 days)[2] times as great as those of the latter. In six removed specimens of aldosteronomas in this study (5-9 days), the mean percent dose/g of ^{131}I-Adosterol is 6 times in the adenomas and 3 times in the adjacent adrenal tissue as great as those of ^{131}I-19-iodocholesterol in the paper reported by Seabold et al.[10], although they did not describe the intervals between the tracer injection

and operation. This higher uptake may relate to earlier visualization. It is preferable to make a diagnosis as early as possible, however more important is, to make a correct diagnosis. The early images (2-4 days postinjection) have some demerits; the background radioactivity produced especially by the liver and the colon is very high and the gallbladder radioactivity may make adrenal definition difficult[39)-41)]. Good quality images could be obtained from the 5 or 6 days postinjection in most cases. If both adrenal radioactivities can be obtained, the judgement of the adrenal images can be made at that time, however unless one or both adrenal (s) are visualized, we must wait at least 7 days or more because the background radioactivity may mask that of the adrenal gland or the adrenal tumor. In my experience, some normal obese subjects showed no or faint visualization of adrenals on the early imaging before 7 days postinjection. The androgen-producing carcinoma could be visualized on 7 days or later imaging.

Although the Pinhole method enabled us to evaluate each adrenal gland morphologically, a satisfactory image could not be obtained from the low radioactive adrenal (Fig. 16). Application of exogenous ACTH to the case of noncortical tumor will produce a more preferable pinhole image.

One major disadvantage of adrenal imaging with ^{131}I-labeled cholesterol is the relatively high radiation dose received by the patient compared to other nuclear imaging procedures, although the gonadal dose is acceptable[42)-44)]. A recently reported ^{123}I-labeled agent, NCL-6-^{123}I[45)], will reduce the radiation dose and produce more suitable pinhole images than ^{131}I-labeled agents.

Conclusions

1) The analysis of the adrenal diverging and pinhole images with ^{131}I-Adosterol was made to establish adrenal imaging patterns, in 43 patients with various adrenal disorders, 4 with adrenal adjacent tumors and one with arrhenoblastoma of the ovary whose images were also included.

2) From this analysis and review of literature, three principles (1. Accumulation in cortical tumors, 2. Relation to endogenous ACTH and 3. Nonaccumulation in noncortical tumors) and several additional factors to make various adrenal imaging patterns with ^{131}I-iodocholesterols could be induced.

3) The accuracy of locating the adrenal tumor-bearing glands was 97% (28/29) with pinhole images and 70% (21/30) with diverging images in baseline conditions.

4) Various adrenal high/low ratios could not be used as confidential indicators to locate the tumor-bearing glands, especially in primary aldosteronism, although the left higher ratios on both views showed high discrepancy between normal and abnormal subjects.

5) The "Pinhole method" is recommended as a simple technique of adrenal imaging, because it provides a high-resolution adrenal image which results in a high diagnostic value. A pinhole collimator is available in any institute which has a gamma camera.

Acknowledgment

This research was conducted under the direction of Prof. Shinji Shinohara. Grateful acknowledgment is made to him for his constant interest and valuable criticism. Thanks are also tendered to the staff of the Department of Radiology, the First, Second and Third Departments of Internal Medicine, the Department of Urology and the Second Department of Pathology for their collaboration.

EXPLANATION OF FIGURES

Fig. 1. Typical adrenal images of primary aldosteronism (Case 9).
The original posterior diverging image (A) shows left lateralization of radioactivity. The left pinhole image reveals a hot nodule at the superior portion of the gland, and a peak formation to confirm it is observed on 90°-rotated 3-dimentional display (B). The right pinhole image and its computer processed display reveal the normality of the gland (C). The scintigraphic findings of the removed left adrenal specimen (D) are consistant with the preoperative findings (B).

Fig. 2. The largest aldosteronoma in this series (Case 12).
A high concentration of the tracer in the right gland and slight radioactivity of the left gland are observed on the diverging image (A). The left pinhole image shows the "cephalopointed oval type" of the normal left gland (B) and a large hot nodule with slight adjacent radioactivity is observed on the right pinhole image (C).

Fig. 3. A slightly asymmetrical case (Case 10).
The diverging image shows right higher asymmetry, which cannot be differentiated from normal asymmetry (A). The left gland shows a normal type on its pinhole image (B). The right pinhole image clarifies the adenoma as a "round high-radioactive area" at the inferior portion of the gland (C). This is consistant with the finding of the adrenal venography (D).

Fig. 4. The smallest aldosteronoma in this series (Case 14).
Both glands are almost equal in radioactivity on the diverging image and the tumor-bearing gland cannot be determined (A). The left pinhole image and its computer processed display (B) clarify a hot nodule at the superior portion of the gland. The right gland is shown as a normal type (C). The T./Ajd. ratio of the removed left specimen is 0.41.

Fig. 5. Idiopathic aldosteronism (Case 18).
The diverging image (A) shows left slightly higher asymmetry. Both glands are delineated as normal types respectively on their pinhole images (B; left, C; right).

Fig. 6. Cushing's adenoma (R.T., a 34-year-old female).
Left intense unilateral visualization is observed on the diverging image (A). A round hot nodule alone is visualized on the left pinhole image (B) which is supported by the findings of the removed left specimen (C, D).

Fig. 7. Cushing's hyperplasia (M.F., a 39-year-old female).
Right higher asymmetry is observed on the diverging image (A). Each adrenal gland shows normal configuration on its pinhole image (B; left, C; right).

Fig. 8. Cushing's hyperplasia (N.O., a 5-year-old male).
Bilateral very intense visualization is demonstrated on the diverging image (A). Both adrenals are delineated as having swelling triangular appearances on their pinhole images respectively (B; left, C; right).

Fig. 9. Cushing's hyperplasia after a left adrenalectomy due to an adenoma (K.T., a 16-year-old female).
Right intense unilateral visualization on the diverging image (A) cannot differentiate hyperplasia from an adenoma. Its cause can be determined to be hyperplasia by the morphological appearance on the pinhole image (B).

Fig. 10. Cushing's carcinoma (F.I., a 14-year-old female).
Right unilateral visualization on the diverging image (A) is represented as a cap-like configuration on its pinhole image (B). Comparing the scintigram of the removed tumor ($7.0\times6.0\times5.5\ cm^3$ in size) with its pathological findings reveals that the well differentiated carcinomatous part was visualized as hot and the undifferentiated part, as cold (C).

Fig. 11. Adrenogenital syndrome due to congenital adrenal hyperplasia (K.O., a 15-year-old female).
A right higher asymmetrical uptake is observed on the diverging image (A). Both glands are delineated as having swelling triangular configuration on their pinhole images (B; left, C; right).

Fig. 12. Adrenogenital syndrome due to a carcinoma (K.K., a 34-year-old female).
A diffuse lower deposit in the left abdominal region and a hot deposit of the right gland are observed on the diverging image (A). The pinhole image exhibits the normality of the right gland (B).

Fig. 13. A large pheochromocytoma of the right gland (N.K., a 53-year-old male).
Unilateral visualization is noted due to lack of the right adrenal radioactivity caused by a large malignant pheochromocytoma.

Fig. 14. A pheochromocytoma located at the periphery of the right adrenal (M.A., a 36-year-old female).
A right higher asymmetrical uptake is observed and the affected gland cannot be determined on the diverging image (A). The right pinhole image (C) shows a defect of radioactivity at the inferior portion of the right gland caused by a benign tumor ($4.0\times3.5\times3.0\ cm^3$ in size). The left gland is visualized as a normal oval type (B).

Fig. 15. A pheochromocytoma centrally located in the right gland (T.U., a 63-year-old male).
The total radioactivity of the right is slightly higher than the left and the affected gland cannot be determined on the diverging image (A). The pinhole images clarify the normality of the left (B) and a cold area in the right (C). The imaging findings of the removed specimen bearing a benign tumor ($3.0\times3.0\times1.8\ cm^3$ in size) (D), are consistant with the preoperative findings (C).

Fig. 16. A left metastatic adrenal tumor (N.K., a 63-year-old male).
The left gland is visualized faintly on the diverging image (A). A cold area surrounded by faint radioactivity is demonstrated on its pinhole image (B) which agrees with a left adrenal tumor about 3 cm in diameter on the CT (D, arrowhead). The right adrenal gland has no intrinsic abnormality, although its inferior lateral margin shows concavity probably due to the right renal cyst (C).

Fig. 17. The smallest metastatic tumor of the right gland (S.K., a 52-year-old male).
On the diverging image (A), the left higher asymmetrical uptake is observed, which suggests the abnormality of either gland. The left gland shows a normal oval type on its pinhole image (B). The right gland has a defect (arrowheads) at its superior portion due to a tumor (1.5×1.5×1.7 cm^3 in size) (C).

Fig. 18. Bartter's syndrome (T.M., a 15-year-old male).
The right higher asymmetrical uptake is observed on the diverging image (A). Both glands show normal types on their pinhole images (B; left, C; right).

Fig. 19. Adrenocortical insufficiency.
A: The diverging image of a patient with prolonged administration of corticosteroids for the treatment of sarcoidosis (Y.M., a 42-year-old female). Both glands are visualized faintly.
B: The diverging image of a patient with Addison's disease (N.T., a 57-year-old female). Both glands are not visualized.

Fig. 20. Pressure effect due to a splenic cyst (K.T., a 42-year-old male).
The left adrenal gland is located considerably lower than the right (A). The superior lateral margin of the left gland shows concavity due to the pressure effect of the splenic cyst (B). The right gland is normal in shape and radioactive distribution (C).

Fig. 21. Pressure effect due to a right renal cyst (K.K., a 66-year-old male).
The right gland is located higher than the left (A). The left gland shows a normal type (B), however the right gland has the pressure effect at its inferior lateral portion due to the right renal cyst (C).

Fig. 22. An arrhenoblastoma of the ovary (M.M., a 21-year-old female).
The anterior diverging image reveals a deposit in the lower abdomen beside both adrenal radioactivities (A). Two hot areas are demonstrated on the multiparallel lower abdominal image (B). The removed tumor (C) is an arrhenoblastoma of the left ovary whose image (D) is the same as the preoperative image (B).

References

1) Beierwaltes, W.H., Lieberman, L.M., Ansari, A.N. and Nishiyama, H.: Visualization of human adrenal gland in vivo by scintillation scanning. J.A.M.A., 216: 275—277, 1971
2) Kojima, M., Maeda, M., Ogawa, H., Nitta, K. and Ito, T.: New adrenal scanning agent. J. Nucl. Med., 16: 666—668, 1975
3) Sarkar, S.D., Beierwaltes, W.H., Ice, R.D., Basmadian, G.P., Hetzel, K.R., Kennedy, W.P. and Manson, M.M.: A new and superior adrenal scanning agent, NP-59. J. Nucl. Med., 16: 1038—1042, 1975
4) Lieberman, L.M., Beierwaites, W.H., Conn, J.W., Ansari, A.N. and Nishiyama, H.: Diagnosis of adrenal disease by visualization of human adrenal gland with ^{131}I-19-iodocholesterol. N. Eng. J. Med., 285: 1387—1393, 1971
5) Conn, J.W., Morita, R., Cohen, E.L., Beierwaltes, W.H., McDonald, W.J. and Herwig, K.R.: Primary aldosteronism, photoscanning of tumors after administration of ^{131}I-19-iodocholesterol. Arch. Intern. Med., 129: 417—425, 1972
6) Moses, D.C., Schteingart, D.E., Sturman, M.F., Beierwaltes, W.H. and Ice, R.D.: Efficacy of radiocholesterol of the adrenal glands in Cushing's syndrome. Surg. Gynecol. Obstet., 139: 201—204, 1974
7) Sturman, M.F., Moses, D.C., Beierwaltes, W.H., Harrison, J.S., Ice, R.D. and Dorr, R.P.: Radioiodocholesterol adrenal images for the localization of pheochromocytoma. Surg. Gynecol. Obstet., 138: 177—180, 1974
8) Conn, J.W. and Cohen, E.L.: Versatility of adrenal photoscanning, diagnosis of unilateral adrenal failure. Arch. Intern. Med., 131: 554—557, 1973
9) Fukuchi, S., Nakajima, K., Takenouchi, T., Nishisato, K., Nakamura, M. and Ogawa, H.: Diagnosis of adrenal disease by visualization of human adrenal glands with ^{131}I-19-iodocholesterol, Jap. J. Nucl. Med., 11: 553—559, 1974
10) Seabold, J.E., Cohen, E.L., Beierwaltes, W.H., Hinermann, D.L., Nishiyama, R.H., Bookstein, J.J., Ice, R.D. and Balachandran, S.: Adrenal imaging with ^{131}I-19-iodocholesterol in the diagnostic evaluation of patients with aldosteronism. J. Clin. Endocrinol. Metab., 42: 41—51, 1976
11) Moses, D.C., Beierwaltes, W.H and Sturman, M.F.: Adrenal imaging in children with ^{131}I-labeled cholesterol. J. Nucl. Med., 14: 634, 1973
12) Troncone, L., Galli, G., Salvo, D., Barbarino, A., Bonomo, L.: Radioisotopic study of the adrenal glands using ^{131}I-19-iodocholesterol. Brit. J. Radiol., 50: 340—349, 1977

13) Kamoi, I., Watanabe, K., Nakayama, C., Morita, K., Koga, I. and Matsuura, K.: Clinical studies on adrenal scintigraphy. Nipp. Act. Radiol., 36: 993—1005, 1976
14) Okuyama, T., Shibuya, H. and Suzuki, S.: Evaluation of diagnostic value of adrenal scintiscanning and venography. Nipp. Act. Radiol., 35: 1098—1106, 1975
15) Rifai, A., Beierwaites, W.H., Feitas, J.E. and Grekin, R.: Adrenal scintigraphy in low renin essential hypertension. Clin. Nucl. Med., 3: 282—286, 1978
16) Ryo, U.Y., Johnston, A.S., Kim, I. and Pinsky, S.M.: Adrenal scanning and uptake with ^{131}I-6-iodomethyl-norcholesterol. Radiology, 128: 157—161, 1978
17) Freitas, J.E., Grekin, R.J., Thrall, J.H., Gross, M.D., Swanson, D.P. and Beierwaltes, W.H.: Adrenal imaging with iodomethyl-norcholesterol (I-131) in primary aldosteronism. J. Nucl. Med., 20: 7—10, 1979
18) Thrall, J.H., Freitas, J.E. and Beierwaltes, W.H.: Adrenal scintigraphy. Seminars in Nucl. Med., 8: 23—41, 1978
19) Sugawara, S., Nakamura, M., Sawai, Y. and Fukuchi, S.: Diagnostic evaluation of the adrenal scanning using ^{131}I-Adosterol. Jap. J. Nucl. Med., 15: 1155—1163, 1978
20) Nishimura, T. and Kimura, K.: Clinical studies of adrenal scintigraphy with ^{131}I-Adosterol. Jap. J. Nucl. Med., 16: 243—250, 1979
21) Nakajo, M., Higuchi, K., Sakata, H., Shinohara, S. and Sonoda, K.: Adrenal scintigraphy using a pinhole collimator. Nipp. Act. Radiol., 38: 340—353, 1978
22) Nakajo, M.: Adrenal imaging with ^{131}I-Adosterol (NCL-6-^{131}I) by Diverging and Pinhole methods, I. analysis of normal adrenal images. Nipp. Act. Radiol., 41: 985—997, 1981
23) Nakajo, M., Ito, T., Shinohara, S., Kawabata, T., Ohi, Y. and Yonezawa, S.: A case of Cushing's syndrome due to adrenal carcinoma —with special reference to ACTH stimulating adrenal scintigraphy—. Jap. J. Clin. Radiol., 23: 977—980, 1978
24) Nakajo, M., Sakata, H. and Shinohara, S.: Positive imaging of arrhenoblastoma of the ovary with ^{131}I-Adosterol: case report. Radioisotopes, 27: 407—409, 1978
25) Nakajo, M., Higuchi, K., sonoda, K. and Shinohara, S.: Clinical study of adrenal scintigraphy with ^{131}I-19-cholesterol —with reference to analysis of normal adrenal scintigram—. Jap. J. Clin. Radiol., 22: 97—102, 1977
26) Forman, B.H., Antar, M.A., Touloukian, R.J., Mulrow, P.J. and Genel, M.: Localization of a metastatic adrenal carcinoma using ^{131}I-19-iodocholesterol. J. Nucl. Med., 15: 332—334, 1974
27) Chatal, J.F., Charbonnel, B., Le Mevel, B.P. and Guihard, D.: Uptake of ^{131}I-19-iodocholesterol by an adrenal cortical carcinoma and its metastases. J. Clin. Endocrinol. Metab., 43: 248—251, 1976
28) Watanabe, K., Kamoi, I., Nakayama, C., Kago, I. and Matsuura, K.: Scintigraphic detection of hepatic metastases with ^{131}I-labeled steroid in recurrent adrenal carcinoma: case report. J. Nucl. Med., 17: 904—906, 1976
29) Gordon, L., Mayfield, R.K., Levine, J.H., Lopes-Virella, M.F., Sagel, J. and Buse, M.G.: Failure to visualize adrenal glands in a patient with bilateral adrenal hyperplasia. J. Nucl. Med., 21: 49—51, 1980
30) Wieland, D.M., Swanson, D.P., Brown, L.E. and Beierwaltes, W.H.: Imaging the adrenal medulla with an I-131-labeled antiadrenergic agent. J. Nucl. Med., 20: 155—158, 1979
31) Korobkin, M., White, E.A., Kressel, H.Y., Moss, A.A. and Montagne, J.P.: Computed tomography in the diagnosis of adrenal disease. A.J.R., 132: 231—238, 1979
32) Leonard, J.M., Rudd, T.G., Burgress, E.C. and Monda, G.A.: Concentration of radiolabeled cholesterol in a feminizing adenoma of the testis. J. Nucl. Med., 20: 307—309, 1979
33) Carpenter, P.C., Wahner, H.W., Salassa, R.M. and Duick, D.S.: Demonstration of steroid-producing gonadal tumors by external scanning with the use of NP-59. Mayo. Clin. Proc., 54: 332—334, 1979
34) Goodman, D.S.: Cholesterol ester metabolism. Physiol. Rev., 45: 747—839, 1965
35) Morita, R., Lieberman, L.M., Beierwaltes, W.H., Conn, J.W., Ansari, A.N. and Nisiyama, H.: Percent uptake of ^{131}I radioactivity in the adrenal from radioiodinated cholesterol. J. Clin. Endocr., 34: 36—43, 1972
36) Koral, K.F. and Sarkar, S.D.: An operator independant method for background subtraction in adrenal uptake measurements: concise communication. J. Nucl. Med., 18: 925—928, 1977
37) Fujita, T., Fukunaga, M., Mukai, T., Yamamoto, I., Dokoh, S., Ishii, Y., Morita, R., Torizuka, K. and Kawamura, J.: Measurement of percent uptake in the adrenal glands with ^{131}I-Adosterol. Jap. J. Nucl. Med., 17: 219—227, 1980
38) Couch, M.W. and Williams, C.M.: Comparison of 19-iodocholesterol and 6-iodomethylnorcholesterol as adrenal scanning agents: J. Nucl. Med., 18: 724—727, 1977
39) Harbert, J.C., Canary, J.J. and Sandock, K.K.: Gallbladder visualization in adrenal scanning: case report. J. Nucl. Med., 17: 33—35, 1976
40) Brown, M.L., Wahner, H.W., Hay, I.D., Hammell, T.C. and Gray, J.E.: Adrenal scintigraphy: comparison of the Anger tomographic scanner and the large-fleld gamma camera: concise communication. J. Nucl. Med., 21: 729—732, 1980

41) Fukunaga, M., Fujita, T., Doko, S., Yamamoto, I., Morita, R., Torizuka, K., Kono, T., Imura, H. and Nakano, Y.: Study of adrenal scintigraphy using PHO/CON (multiplane tomographic scanner). Jap. J. Nucl. Med., 17: 355—361, 1980
42) Kirschner, A.S., Ice, R.D. and Beierwaltes, W.H.: Radiation dosimetry of ^{131}I-19-iodocholesterol. J. Nucl. Med., 14: 713—717, 1973
43) Ice, R.D., Kircos, L.T., Coffey, J.L., Watson, E., Sarkar, S.D. and Beierwaltes, W.H.: Radiation dosimetry of I-131-6-iodomethylnorcholesterol. J. Nucl. Med., 17: 540, 1976 (abst.)
44) Carey, J.E., Thrall, J.H., Freitas, J.E. and Beierwaltes, W.H.: Absorbed dose to the human adrenals from iodo methylnorcholesterol (I-131) "NP-59": concise communication. J. Nucl. Med., 20: 60—62, 1979
45) Kamoi, I., Oshiumi, Y., Tateno, Y., Shishido, F., Ido, T., Suzuki, K., Irie, T., Fukushi, K., Nakayama, C., Matsuura, K., Itoh, T., Ogawa, H., Maeda, M. and Kojima, M.: Adrenal scintigraphy using ^{123}I labeled 6β-iodomethyl-19-norcholest-5(10)-en-3β-01 (NCL-6-^{123}I). Jap. J. Nucl. Med., 17: 389—393, 1980